The annealing effect on microstructure and ESR properties of (Cu/Ni) co-doped ZnO nanoparticles

A. Guler[a], L. Arda[b,*], N. Dogan[c], C. Boyraz[d], E. Ozugurlu[e]

[a] Marmara University, Ataturk Faculty of Education, Department of Computer Education and Instructional Technologies, 34722 Goztepe, Istanbul, Turkey
[b] Bahcesehir University, Faculty of Engineering and Naturel Sciences, Department of Mechatronic Engineering, 34349, Besiktas, Istanbul, Turkey
[c] Gebze Technical University, Faculty of Science, Department of Physics, 41400, Gebze, Kocaeli, Turkey
[d] Marmara University, Faculty of Technology, Department of Mechanical Engineering, 34722, Goztepe, Istanbul, Turkey
[e] Istanbul Technical University, Faculty of Science and Arts, Department of Mathematical Engineering, 34467, Maslak, Istanbul, Turkey

ARTICLE INFO

ABSTRACT

$Zn_{0.94}Cu_{0.01}Ni_{0.05}O$ nanoparticles were synthesized by sol-gel technique and annealed under varying wide temperature range (450, 500, 550, 600, 700, 800, and 900 ^{0}C). Differential thermal analysis (DTA), and thermo gravimetric analysis were performed using a wide temperature range with optimizing the annealing temperature and clarifying the possible weight losses. The structural variation of nanoparticles with dopant ratio and annealing temperature were studied by X-ray diffraction technique and we found that the nanoparticles annealed at 450, 500 and 550 °C were optimum annealing temperatures with the property of single phase with ZnO wurtzite hexagonal structure. Above 550 °C, two phases were observed, namely ZnO and NiO. A slight temperature dependent less structural distortion was revealed with NiO phase especially after the sample annealed at 550 °C. The microstructural parameters were also presented. Cluster shape random agglomeration was observed in all frames of SEM images obtained by different annealing temperatures. Detailed Electron Spin Resonance (ESR) measurements were performed to reveal the magnetic behaviour of all nanoparticles.

1. Introduction

The variety of Zinc oxide (ZnO) doped compounds with varying elements becomes interesting and important due to offering controllable fascinating physical and chemical properties [1–5]. The discovered electronic properties of ZnO and ZnO–based semiconductors have an importance in broad range industrial application areas such as spintronics, optoelectronics, biomaterials, cosmetics, varistors, and surface acoustic wave devices [6–15]. Controlling sizes and shapes using varying synthesizing methods also give an extra opportunity for band-gap engineering by adjusting band-gap energies [16–21]. With 3.37 eV wide band-gap and 60 meV large exciton binding energy, potential dilute magnetic semiconductor (DMS) material ZnO is widely used in industry for the fabrication of optoelectronic devices [22].

Knowing the properties of vacancies and defects is crucial for device production since they provide variety of diffusion mechanisms. It is well known that to optimize the electrical, magnetic, and optical properties of ZnO which strongly depend on the impurities and defects in ZnO materials, some certain elements are needed to be added into ZnO. Therefore, especially for versatile applications, the potential interest for wide band-gap oxide semiconductors doping with transition metal (TM) ions (Ni, Fe, Mn, Cu and Co) has been increasing [23]. The study by Duru et al. [24] revealed the physical origins of room temperature ferromagnetism in Cr doped ZnO. As predicted theoretically, in Ni doped ZnO, some effects have been observed regarding the room temperature (RT) ferromagnetism [25,26]. The reports on TM-doped ZnO in the literature emphasize that TM-doped ZnO family would be a suitable candidate to achieve Curie temperature above RT [27–29]. With the property of having a near radius to Zn (0.60 Å), Nickel (0.69 Å) element is known as one of the important dopant elements affecting magnetic and luminescence properties ZnO [30–32].

In Arda et al. [33] and the references therein, it was stated that the oxygen vacancies and the interstitial Zn defects play an important role in the ferromagnetic behaviour in Co doped ZnO.

Since Cu has a deep level impurity and Ni gives a RT ferromagnetism, Cu/Ni doped ZnO is an interesting material. However, only a few studies have been done on photoluminescence properties of Cu/Ni doped ZnO nanoparticles [34,35]. The Electron Spin Resonance (ESR) also has not been studied yet to analyse the magnetic properties of Cu/Ni-doped ZnO nanoparticles. In the literature, varying

synthesizing methods, conditions, and dopant elements affect the resultant magnetic properties and some certain points of magnetic properties are needed to be clarified with varying techniques and these are still the matter of discussion.

In the present paper, Cu and Ni co-doped ZnO nanoparticles were synthesized using sol-gel method. The effect of annealing temperature on structural and morphological of nanoparticles was investigated. Furthermore, a detailed microstructural parameter calculation was presented. To identify and study the defects in ZnO materials, the researchers used the ESR which is well known among the experimental techniques.

The ESR is used for the first time to choose and support the best sample among the annealed samples' set with varying temperature to analyse the magnetic properties of Cu/Ni doped ZnO.

2. Experimental procedure

As polycrystalline form, $Zn_{0.94}Cu_{0.01}Ni_{0.05}O$ nanoparticles were synthesized using sol-gel technique and annealed with wide temperature range from 450° to 900°C. In this synthesizing process, the chemicals related to the composition zinc acetate dehydrate, nickel acetate tetra hydrate and copper acetate tetra hydrate were used as precursor materials. To prepare clear homogenous solutions, methanol and acetyl acetone were used. All the materials were weighed and mixed with a magnetic stirrer at RT. After this process, the solutions were removed from the solvent and preheated at 200–350 °C for 10 min under air, for details see [1,4,36,37].

Finally, in a programmable step furnace, heat treatment procedure with a wide temperature range (450, 500, 550, 600, 700, 800, and 900 ^{0}C) was applied for each sample separately to obtain the desired phases and physical properties. The thermal behaviour of the $Zn_{0.94}Cu_{0.01}Ni_{0.05}O$ xerogel was clarified by differential thermal analysis (DTA) and thermo gravimetric analysis techniques by means of (TG)/SII 7300 Exstar thermal analyser system in the air with a heating rate of 10 °C/min. The structural phase definition was provided by X-Ray diffraction measurement technique (Rigaku diffractometer) for synthesized nanoparticles with Cu K_α radiation source. By means of JEOL, JSM-5910LV model Scanning Electron Microscope (SEM) tool, the surface morphology images were monitored to figure out the microstructural properties.

ESR spectra of $Zn_{0.94}Cu_{0.01}Ni_{0.05}O$ (ZnCuNiO) (annealed at 450, 500, 550, 600, 700, 800, and 900 ^{0}C) nanoparticles were collected at RT using a Jeol Mark-JES-FA300 Series ESR X-band (ν = 9.4 GHz) spectrometer equipped by an electromagnet which provides a DC magnetic field up to 2T. The static magnetic field was varied in the range of 0–1000 mT. All the samples were loaded into quartz ESR tubes and the magnetic contributions of the cavity and quartz tubes were extracted from measurements.

3. Results and discussions

3.1. Structural analysis

The prepared ZnCuNiO xerogel nanoparticles by sol-gel technique were analysed by DTA and TG measurement techniques to determine the thermal behaviours and the possible weight loses with increasing temperature in Fig. 1. Evaporation of volatile organic component and the removal of solvent were observed at 100 °C the first 23% temperature-dependent weight decrease effect; in that temperature, a sharp and strong endothermic was revealed in Fig. 1. On the same figure, looking at the DTA curve, two small interval endothermic and a wide exothermic peak were depicted in the temperature range between 125 and 360 °C in which region the evaporation of the volatile organic component and the removal of the residual solvent were observed as 55% which was a high level of the second weight decrease in TG curve. After ending with two small endothermic peaks around 360 °C, carbon-
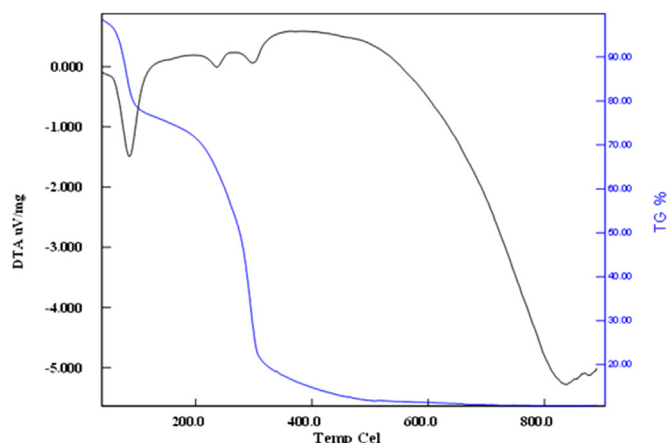

Fig. 1. The DTA and TG curves for the $Zn_{0.94}Cu_{0.01}Ni_{0.05}O$ nanoparticles obtained by sol-gel solution at RT in air for 3 days.

based materials were burned out until 650 °C. In 360–650 °C temperature region, the third weight lose with 20% was observed in TG curve.

The structural and magnetic properties of the resulting undoped ZnO and transition metals doped ZnO dominantly depend on the synthesizing conditions [1]. To reveal crystal structure properties and the possible phases, X-ray diffraction of ZnCuNiO samples annealed at 450, 500, 550, 600, 700, 800, and 900 °C were performed for $20° \leq 2\Theta \leq 80°$ range as shown in Fig. 2a. Samples annealed at 450, 500, and 550 °C exhibit the same peaks without any secondary phase in Fig. 2b. However, the samples (as seen in Fig. 2a) annealed at 600 °C and above, show NiO peaks which was also exhibited by Rietveld analysis in Fig. 2c for the sample annealed at 600 °C. We conclude that up to 550 °C there is an optimum annealing temperature for ZnCuNiO nanoparticles and the peaks in all patterns match with the hexagonal ZnO lattice with the space group of *P63mc*. The average particle size (D) was determined by the Debye-Sherrer Eq. (1):

$$D = \frac{K\lambda}{\beta Cos\theta} \tag{1}$$

where β is the intensity at the full width at the half-maximum (FWHM) and θ is the angle of Bragg diffraction, K and X-ray wavelength λ constants are 0.9 and 0.15406 nm, respectively. The variations of average particle sizes with concentration are exhibited in Table 1. The structural distortion was prevented by partially replacing the dopant elements Cu^{2+} (0.73 Å) and Ni^{2+} (0.69 Å) with Zn^{2+} (0.60 Å) and this replacing showed an increase in average particle sizes as presented in Table 1.

In Fig. 3, the unit cells of ZnO at various temperatures and the crystal structure of ZnCuNiO are given. VESTA visualization package is preferred to illustrate the unit cell of hexagonal ZnO (Fig. 3a), and randomly %5 Ni and %1 Cu doped to ZnO super cell (Fig. 3b) by experimentally obtained parameters which are also indicated in Table 1.

With the help of the XRD pattern and Eq. (2), the lattice parameters a and c were calculated:

$$\frac{1}{d_{hkl}^2} = \frac{4}{3}\left(\frac{h^2+hk+k^2}{a^2}\right) + \frac{l^2}{c^2} \tag{2}$$

The unit cell of the hexagonal system volume (V) was calculated from the Eq. (3):

$$V = 0.866 \quad a^2c \tag{3}$$

The lattice parameters a and c are plotted versus temperature T for ZnCuNiO nanoparticles in Fig. 4a and b, respectively. Cu^{2+} and Ni^{2+} replace Zn^{2+} substitutionally yielding ZnCuNiO single phase system up to 550 °C. In Fig. 4b, until 550 °C out of plane c lattice parameter increases, which shows a single phase and after 550 °C this single phase
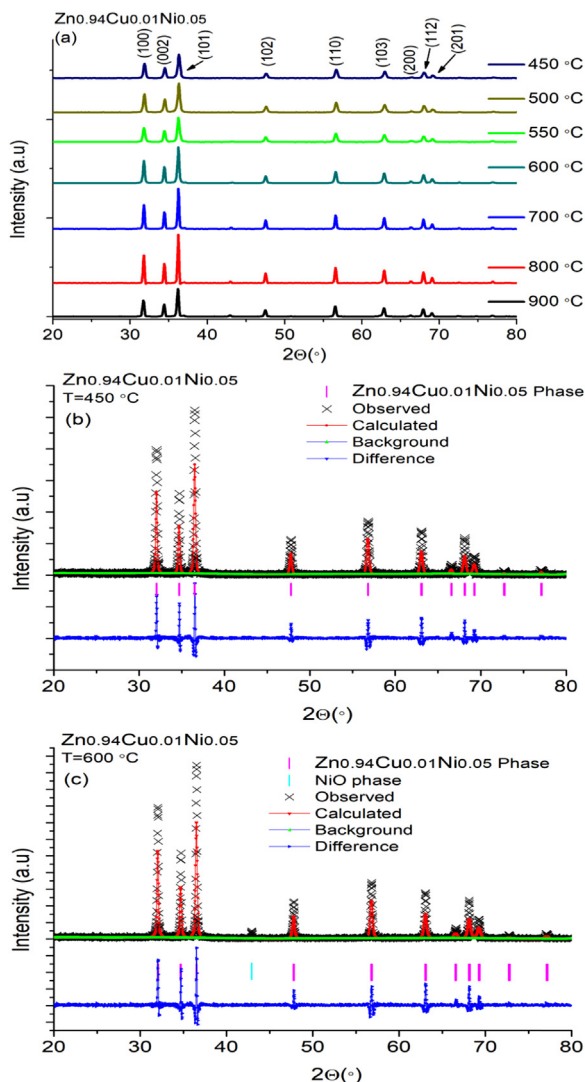
Fig. 2. X-ray diffraction of $Zn_{0.94}Cu_{0.01}Ni_{0.05}O$ samples annealed at a wide temperature region (450, 500, 550, 600, 700, 800, and 900 °C) in (a), and Rietveld analysis of $Zn_{0.94}Cu_{0.01}Ni_{0.05}O$ samples annealed at 450, and 600 °C in (b) and (c) respectively.

Table 1

The variation of lattice parameters, average particle sizes, and volume of the unit cell with temperature dependency.

Temperature (°C)	D (nm)	a(Å)	c(Å)	c/a	Volume, V (Å³)
450	22.91	3.243	5.197	1.602	47.333
500	24.58	3.250	5.203	1.601	47.592
550	26.13	3.245	5.211	1.606	47.519
600	26.96	3.252	5.205	1.601	47.669
700	29.86	3.252	5.201	1.599	47.632
800	32.15	3.248	5.201	1.601	47.515
900	33.45	3.242	5.186	1.600	47.203

disappears and the c lattice parameter decreases as the annealing temperature increases. In a structure, two main reasons, namely doping ratio and annealing temperature, are predominantly affecting stress and strain. Therefore, stress (σ) and microstrain (ε) were calculated by Eq. (4) and Eq. (5). These parameters were presented in Table 2.

$$\sigma = -453.6 \times 10^9 \left(\frac{c - c_0}{c_0} \right) \tag{4}$$

$$\varepsilon = (\beta_{1/2} \cos\theta)/4 \tag{5}$$

In Eq. (4), c_0 and c values belong to the lattice constant in unstrained ZnO and out of plane lattice parameters of $Zn_{0.94}Cu_{0.01}Ni_{0.05}O$ samples, respectively. As presented in Table 2, σ values with negative signs address compressive stress, which is opposite to tensile stress. In Eq. (5), θ and β are the Bragg's diffraction angle and the full width at half maxima (FWHM), respectively. In Fig. 4c, except the sample annealed at 550 °C, we observed that because of the increasing annealing temperature strain (ε) decreases and stress (σ) increases.

In Fig. 4d, c/a decreases while the volume increases. As the temperature increases, we noticed a zigzag behaviour in the lattice parameters and the volume of the unit cell. In our samples, the c/a ratio is not the same as the literature value of $c/a = 1.60$ for an ideal ZnO structure Gottstein [38] due the existence of microstrains and defects in the crystal structure.

In the crystal structures, the existing of strain and stress forces may cause an increment in physical defects and dislocations. Therefore, the dislocation density described as the amount of defect in the sample was calculated using Eq. (6) and exhibited in Table 2.

$$\delta = \frac{1}{D^2} \tag{6}$$

As seen in Table 2, a very low dislocation density (δ) is essential for a good crystallinity and the obtained very low δ values are an indication of a good crystallinity in ZnCuNiO nanoparticles. The increasing annealing temperature in ZnCuNiO samples affects the growth of the particle size which is directly an effect of lowering the dislocation density values. The atomic localities and their displacements in ZnCuNiO systems were depicted by the calculated u values;

$$u = \left(\frac{a^2}{3c^2} \right) + \frac{1}{4} \tag{7}$$

where both c and a are the lattice parameters in ZnCuNiO structures. The calculated u values revealed a fluctuation tendency with increasing annealing temperature. The Zn-O bond length L values affected by the doping ratio and heat treatment were calculated by Eq. (8) as follows;

$$L = \sqrt{\left(\frac{a^2}{3} \right) + (0.5 - u)^2 {}^* c^2} \tag{8}$$

From Tables 1 and 2, it can be seen that the lattice parameters (c/a) values and Zn-O bond lengths (L) show completely an inverse behaviour.

The surface particle distribution was monitored for ZnCuNiO nanoparticles annealed at 550, 600, 700, 800 and 900 °C as seen in Fig. 5. The particle sizes and agglomeration increase as the temperature increases. These results are coherent with the calculated data shown in Table 1. Cluster shape random agglomeration was observed in all frames of SEM images obtained by different magnifications as shown in Fig. 5. The composition of the $Zn_{0.94}Cu_{0.01}Ni_{0.05}O$ nanoparticles is analysed by EDS spectrum. Zn, Cu, Ni, and O peaks are obviously seen in EDS spectrum. The contents of Zn, Cu, and Ni are compatible with the synthesized of nanoparticles.

3.2. Magnetic analysis

At the RT, ESR spectra were taken in order to investigate the detail of the magnetic components in the nanoparticles and the results were shown in Fig. 6. The ESR spectra of the ZnCuNiO exhibit a broad single resonance peak. ESR measurements have been performed and analysed through the annealing temperature dependence of the g-factor and the line-widths of peak-to-peak (ΔH_{PP}) of ESR spectra. Experimental X band ESR spectra of ZnCuNiO nanoparticles which annealed at different temperatures recorded at RT are shown in Fig. 6. It is seen that the ESR spectra for 450 °C annealed temperature is dominated by a strong and broadest signal at around 300 mT. Generally, the place of the peak is
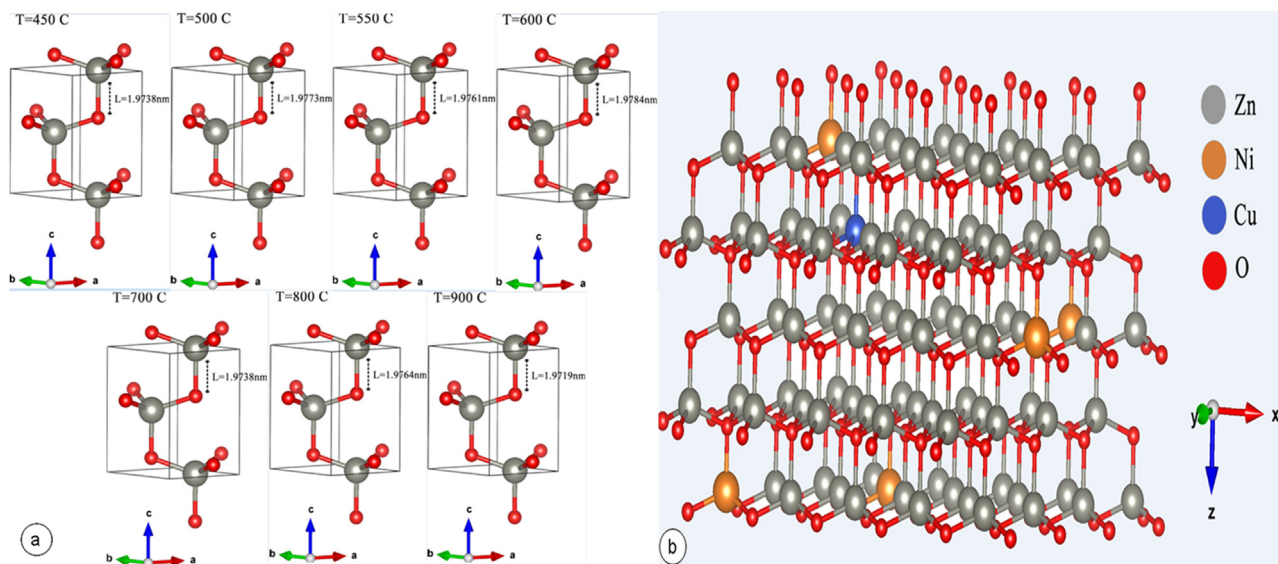
Fig. 3. Illustrations of a) Unit cell of ZnO at various temperatures and b) Crystal structure of $Zn_{0.94}Cu_{0.01}Ni_{0.05}O$ nanoparticles.

stable and the reason of broadness of signal arises due to dipolar interactions and spin-exchange interactions. The intensity of ESR peak changed with the annealed temperature and the highest peak is observed for 450 ^{0}C nanoparticles and the other nanoparticles' peak intensity are shown in Fig. 6. When the annealing temperature is increased, a significant reduction in peak intensity was observed. This may be due to the increasing number of zinc vacancy in the samples.

The asymmetry factor (P_{asy}) values are represented in Table 3 and can be calculated by using the formula

$$P_{asy} = 1 - \frac{h_u}{h_L} \tag{9}$$

where h_U is the height of the absorption peak above the base line and h_L is the height of the absorption peak below the base line of the ESR

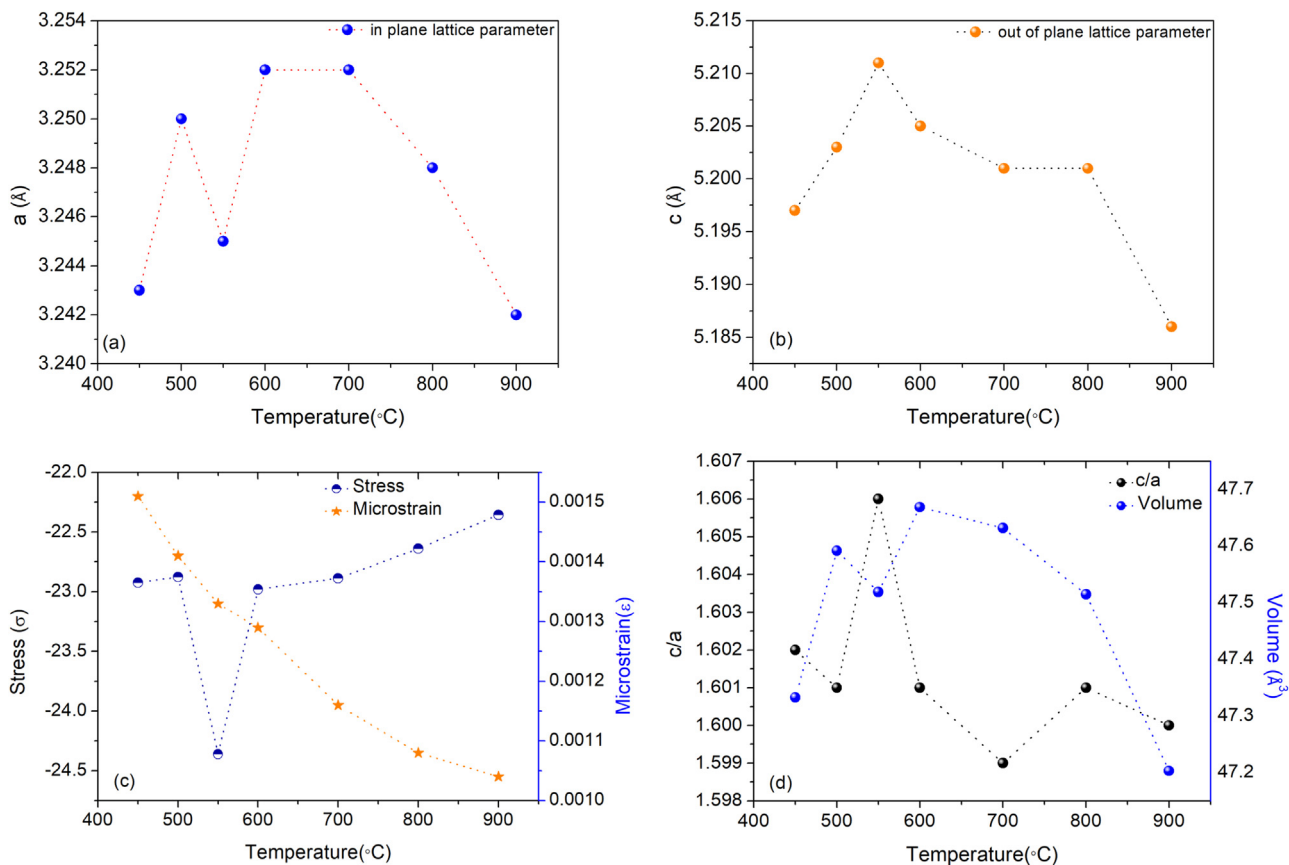Fig. 4. a The lattice parameter *a* versus temperature *T* for $Zn_{0.95-x}Cu_xNi_{0.05}O$ nanoparticles.b The lattice parameter *c* versus temperature *T* for $Zn_{0.95-x}Cu_xNi_{0.05}O$ nanoparticles c Stress (σ) and microstrain ($\mathcal{E}$) versus temperature *T* for $Zn_{0.95-x}Cu_xNi_{0.05}O$ nanoparticles d The lattice parameter c/a and volume versus temperature T for $Zn0.94Cu0.01Ni0.05$ O nanoparticles.

Table 2

The variation of $\mathcal{E}$, σ, δ, u, and L parameters with temperature in $Zn_{0.95-x}Cu_xNi_{0.05}O$ structures.

Temperature (°C)	$\mathcal{E}$	$\sigma * 10^9$ (N/m²)	$\delta * 10^{14}$	u	L (nm)
450	0.00151	− 22.924	0.001906	0.3798	1.9738
500	0.00141	− 22.878	0.001654	0.3800	1.9773
550	0.00133	− 24.360	0.001465	0.3793	1.9761
600	0.00129	− 22.980	0.001375	0.3801	1.9784
700	0.00116	− 22.888	0.001122	0.3803	1.9781
800	0.00108	− 22.639	0.000967	0.3800	1.9764
900	0.00104	− 22.356	0.000894	0.3802	1.9719

spectra. The peak to peak intensity and the peak to peak line-width are calculated from Figs. 6 and 6a. Moreover, the number of spins (N_s) corresponding to unpaired electrons which contribute to the resonance signal Das et al. and the references therein [43] is formulated as

$$N_s = 0.285 \times I_{pp} \times (\Delta H_{pp})^2 \tag{10}$$

Asymmetry parameters were changed randomly with temperature and the maximum value of P_{asy} was observed at 450 °C since the number of spins attains a maximum at 450 °C. Since the number of spin is high, the number of spin between two energy levels will also be high. On the contrary, the observed peak intensity will be high and the line width will be expected narrow.

To understand the relaxation mechanism of the ESR active spins, peak-to-peak line-widths ΔH_{pp} of ESR spectra and g-factor have been analysed. ΔH_{pp} is determined as the width between points of maximum and minimum of the first derivative of the ESR line.

In Fig. 6a, each original ESR spectra curve has 65532 data points,

the simulation curves are obtained by cubic spline interpolation in MATLAB using only 17 data points with the relative errors in the range of 0.0692, 0.126, 0.1558, 0.2122, 0.2882, and 0.1187, for each samples starting 450 up to 900 °C, respectively.

The line-widths of peak-to-peak (ΔH_{pp}) of the ESR signals take different values between 86 and 121 mT when the annealing temperature is changed from 450 °C to 900 °C as shown in Fig. 7.

We calculated the g values of the nanoparticles according to the formula as $h\nu = g\mu_\beta H$,

where h is Planck's constant, ν is the operating frequency which is 9.5 GHz, μ_β (Bohr magneton), and H is the static magnetic field, varied in the range of 0–1000 mT. The calculated g-values were greater than 2 as shown in Table 3 and Fig. 8 which may be due to the Zn vacancy in the structure and this indicated a ferromagnetic behaviour of the ZnCuNiO nanoparticles.

In ZnO materials, the ESR line with g = 1.96 (with the components $g_{\parallel} = 1.957$ and $g_\perp = 1.955$) is usually observed, which is understood as the result of conduction electrons at the surface centre of ZnO particles and donor centres in powder Arda et al. [33]. Moreover, an ESR signal with g-value 1.995 showing singly ionized oxygen vacancies and with g-values between from 2.003 to 2.019 indicating singly ionized zinc vacancy were observed in Taylor [39], Galland [40].

The change of the g-value with respect to the annealing temperature is demonstrated in Fig. 8. The g-value of the signals changes from 2.071 to 2.28, where it reaches the maximum g-value of 2.28 for 550 °C. The g-values increase up to 550 °C, then the g-values do not change much after 550 °C and are almost linearly dependent on the temperature. Moreover, when we look at the crystal structure of ZnO, the doped Cu and Ni ions fill the Zn sites substitutionally up to 550 °C. This is
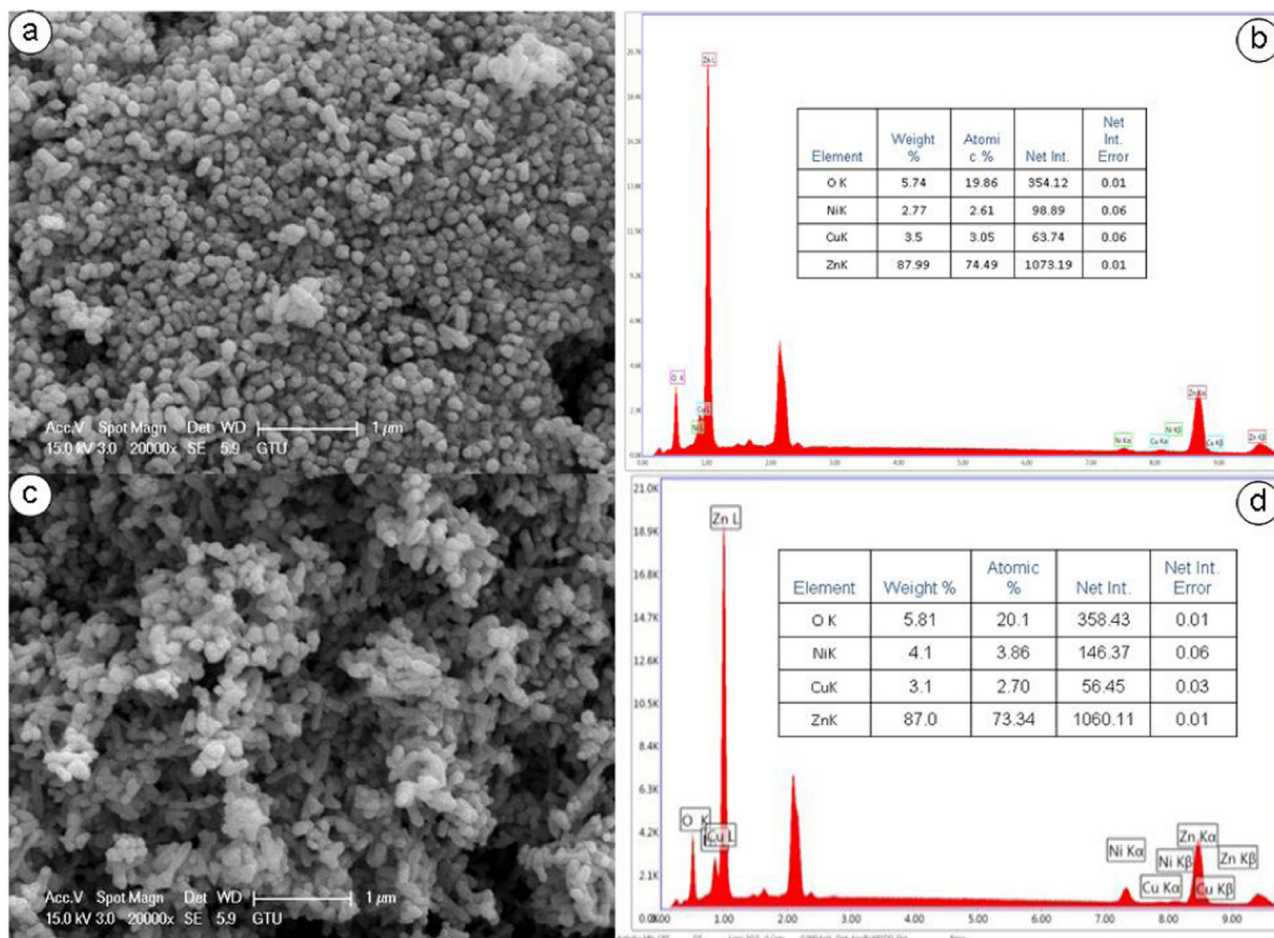

Fig. 5. The SEM images and the EDS results for ZnCuNiO nanoparticles annealed at (a & b) 550 °C, (c & d) 600 °C, (e & f) 700 °C, (g & h) 800 °C and (i & j) 900 °C.
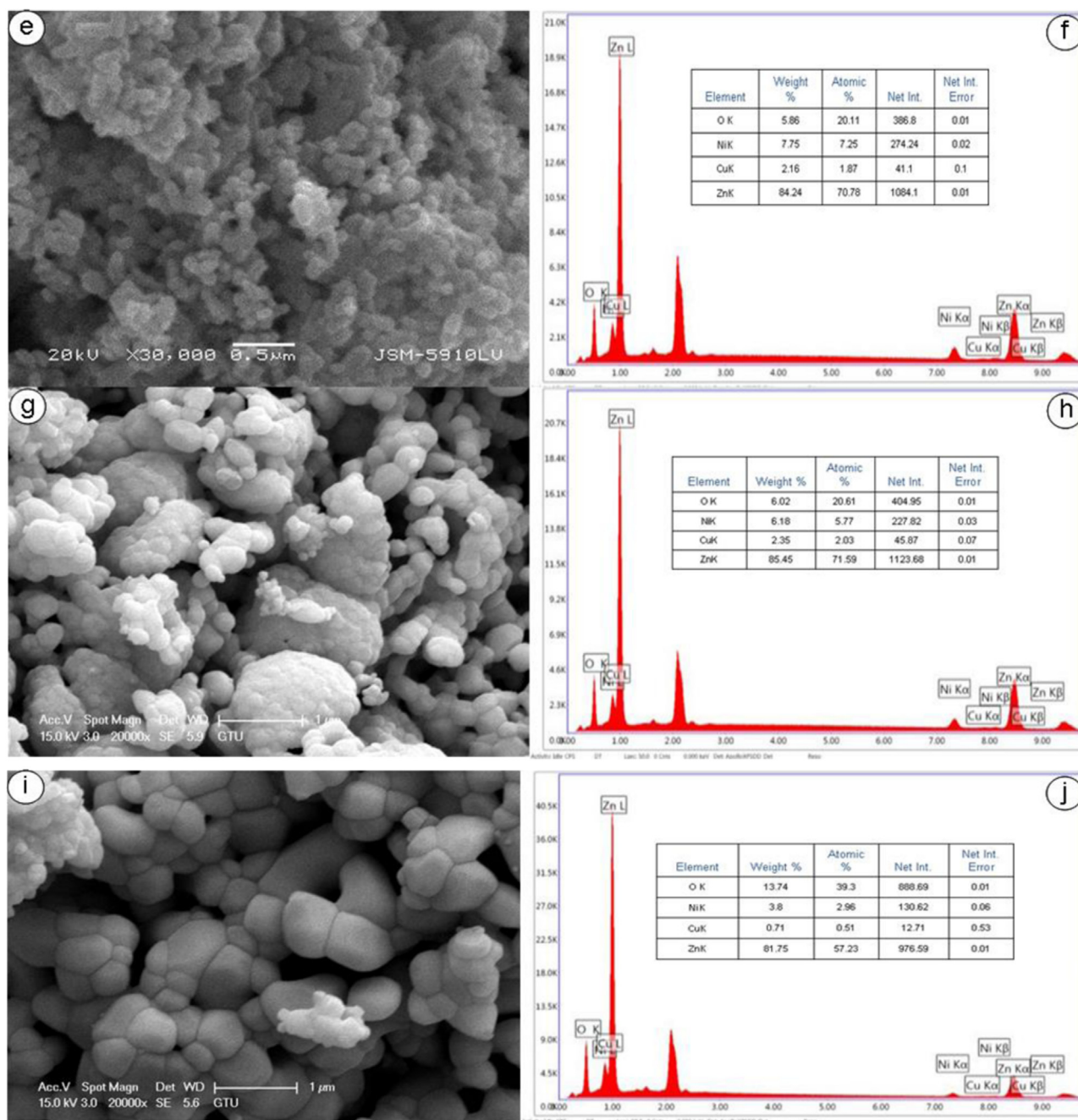
Element	Weight %	Atomic %	Net Int.	Net Int. Error
O K	5.86	20.11	386.8	0.01
NiK	7.75	7.25	274.24	0.02
CuK	2.16	1.87	41.1	0.1
ZnK	84.24	70.78	1084.1	0.01

Element	Weight %	Atomic %	Net Int.	Net Int. Error
O K	6.02	20.61	404.95	0.01
NiK	6.18	5.77	227.82	0.03
CuK	2.35	2.03	45.87	0.07
ZnK	85.45	71.59	1123.68	0.01

Element	Weight %	Atomic %	Net Int.	Net Int. Error
O K	13.74	39.3	888.69	0.01
NiK	3.8	2.96	130.62	0.06
CuK	0.71	0.51	12.71	0.53
ZnK	81.75	57.23	976.59	0.01

Fig. 5. (*continued*)

explained in terms of particle sizes listed in Table 1 and Fig. 2a-c where single phase is observed up to and including 550 ^{0}C. After 550 ^{0}C, NiO secondary phases were observed. That means that Cu and Ni ions do not substitute with Zn sites. At 550 ^{0}C, microstrain ($\mathcal{E}$) has a minimum value of 0.00133. An ideal value for a single position parameter u of $3/8 = 0.375$ is expected and we find u as 0.3793 which is the minimum value very close to the ideal value among the other u values.

The electronic configurations of Cu^{+2} and Ni^{+2} ions are $3d^9$ and $3d^8$, respectively. In general, it is assumed that the cause of ferromagnetism comes from the exchange interaction between the localized d spins on the transition metals and the localized carriers from the valence band.

The broadening of line width is a result of exchange interactions [41]. In addition to this, the existence of Ni in ZnO nanoparticle could improve the magnetic d-d exchange interaction between the magnetic moment Ni^{+2} provide for the ferromagnetic state [42] and the

references therein. In Figs. 6 and 6a, ESR spectra confirm the strong exchange interaction which can be considered as the cause of the RT ferromagnetism in Cu and Ni doped ZnO.

In the literature, there are many studies about RT ferromagnetism in DMSs, however they are lacking of explaining observed ferromagnetism by the existing theories. The ferromagnetic properties of DMSs depend strongly on sample preparation which may contain defects and whether the resulting material is a single phase or not [33]. Some researchers have claimed to observe ferromagnetic behaviour arising only from a secondary phase and not from the material itself. It is known that Cu-related oxides such as CuO, Cu_2O, or Cu clustering could not contribute to the RT ferromagnetism [42]. As shown in Fig. 2, XRD spectra reveal no appearance of CuO peak but the existence of NiO peaks. Presence of the NiO secondary phase would affect the magnetic properties of the ZnCuNiO nanoparticles.
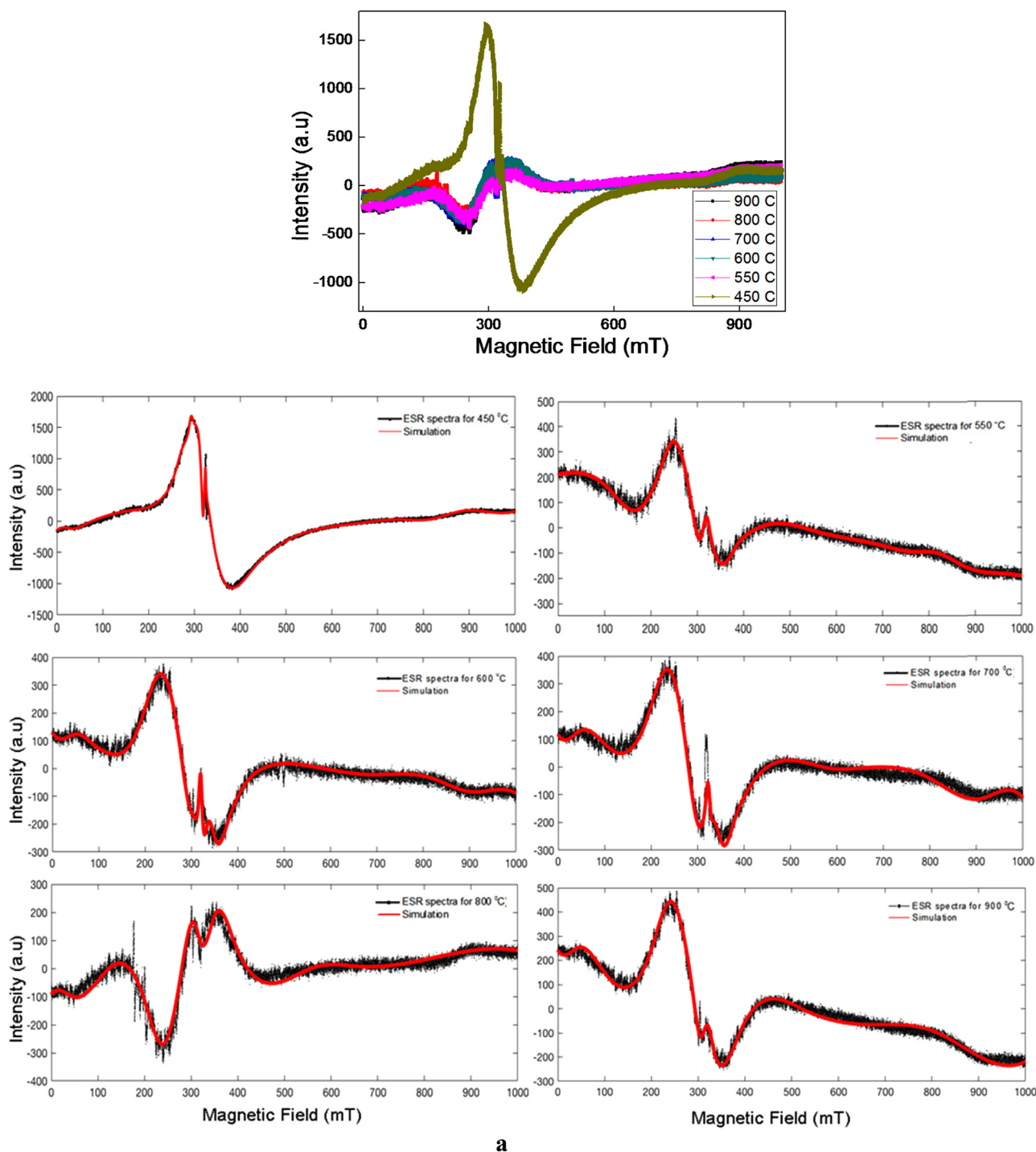
Fig. 6. Experimental X band-ESR spectra of all samples at RT. **a** Experimental X band-ESR spectra of all samples individually (450, 550, 600, 700, 800 and 900 °C) at RT.

4. Conclusion

In nanoparticle form, $Zn_{0.94}Cu_{0.01}Ni_{0.05}O$ nanoparticles were synthesized by sol-gel technique and annealed under varying wide temperature range (450, 500, 550, 600, 700, and 900 °C). Nanoparticles annealed at 450, 500, and 550 °C exhibit the same peaks without any secondary phase and further increment in annealing temperature gave rise to NiO secondary peak. We conclude that up to 550 °C there is an optimum annealing temperature for $Zn_{0.94}Cu_{0.01}Ni_{0.05}O$ nanoparticles and the peaks in all patterns match with the hexagonal ZnO lattice. With the outcomes of very low dislocation density values, we can

conclude that a very good crystallinity in $Zn_{0.95-x}Cu_xNi_{0.05}O$ nanoparticles is observed. Cluster shape random agglomeration was observed in all frames of SEM images obtained by different temperatures. Based on the relaxation mechanism of the ESR active spins, it seems that there is a certain annealing temperature for optimum magnetic properties and ESR g-factor and ΔH_{pp} parameters. It was observed that the ESR spectra for 450 °C annealed temperature was dominated by a strong and broadest signal at around 300 mT. Generally, the place of the peak is stable and the reason of broadness of signal arises due to dipolar interactions and spin-exchange interactions. Cu and Ni doped ZnO nanoparticles exhibiting RT ferromagnetism could be a suitable

Table 3
The ESR parameters Pasy, Ns, I_{pp}, g-value and line-width ΔH_{pp} with various annealing temperatures.

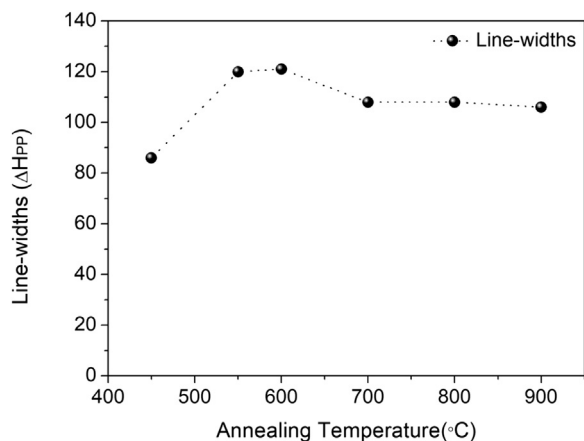| Annealing Temperature (°C)	h_L	h_u	P_{asy}	N_s	I_{pp}	g-values	Line-widths (ΔH_{PP})
450	− 1092.3	1670.7	2.5295	5284	2763	2.07	86
550	− 434.5	170.5	1.3925	2482	605	2.28	120
600	− 375.3	284.7	1.7584	2753	660	2.22	121
700	− 396.9	281.1	1.7083	2253	678	2.21	108
800	− 335.5	237.5	1.708	1904	573	2.27	108
900	− 486.9	254.1	1.522	2372	741	2.23	106

Fig. 7. The annealing temperature dependence of the line-widths (ΔH_{pp}) of ESR spectra of all samples.

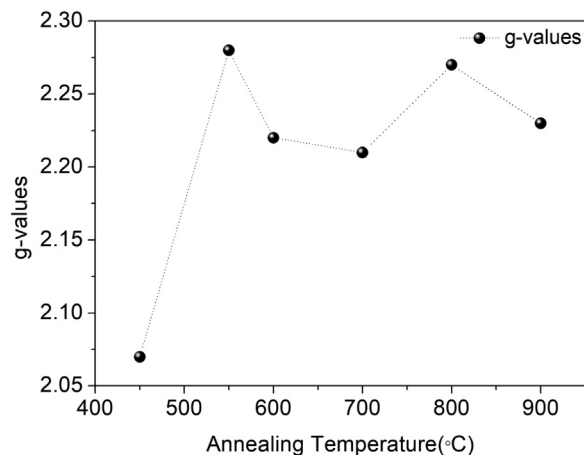**Fig. 8.** The annealing temperature dependence of g-value of all samples.

material for spintronic applications.

Acknowledgements

References

[1] C. Boyraz, N. Doğan, L. Arda, Microstructure and magnetic behaviour of (Mg/Ni) co-doped ZnO nanoparticles, Ceram. Int. 43 (2017) 15986–15991.

[2] E. Asikuzun, A. Donmez, L. Arda, O. Cakiroglu, O. Ozturk, D. Akcan, M. Tosun, S. Ataoglu, C. Terzioglu, Structural and mechanical properties of (Co/Mg) co-doped nano ZnO, Ceram. Inter 41 (2015) 6326–6334.

[3] E. Asikuzun, O. Ozturk, L. Arda, C. Terzioglu, Microstructural and electrical characterizations of transparent Er-doped ZnO nano thin films prepared by sol–gel process, J. Mater. Sci.: Mater. Electron 28 (2017) 14314–14322.

[4] Z.K. Heiba, L. Arda, M.B. Mohamed, M.A. Al-Jalali, N. Dogan, Structural and Magnetic Properties of (Al/Mg) Co-doped Nano ZnO, J. Supercond. Nov. Magn. Volume: 26 (Issue: 11) (2013) 3299–3304.

[5] N. Üzar, G. Algün, N. Akçay, D. Akcan, L. Arda, Structural, optical, electrical and humidity sensing properties of (Y/Al) co-doped ZnO thin films, J. Mater. Sci.: Mater. Electron 28 (2017) 11861–11870.

[6] H. Ohno, Making nonmagnetic semiconductors ferromagnetic, Science 281 (1998) 951–956.

[7] S.A. Wolf, D. Awschalom, R.A. Buhrman, J.M. Daughton, S.V. Molnar, M.L. Roukes, A.Y. Chtchelkanova, D.M. Treger, Spintronics: a spin-based electronics vision for the future, Science 294 (2001) 1488.

[8] T. Dietl, Ferromagnetic semiconductors, Semicond. Sci. Technol. 17 (2002) 377.

[9] D. Ljubas, G. Smoljanic, H. Juretic, Degradation of Methyl Orange and Congo Red dyes by using TiO2 nanoparticles activated by the solar and the solar-like radiation, J. Environ. Manag. 161 (2015) 83–91.

[10] B. Gunjan, S. Rayamajhi, ZnO nanoparticles: a promising anticancer agent, Nanobiomedicine 3 (2016) 9.

[11] Y. Ammaih, A. Abderrazak, B. Hartiti, A. Ridah, P. Thevenin, M. Siadat, Structural, optical and electrical properties of ZnO: Al thin films for optoelectronic applications, Opt. Quant. Electron. 46 (2014) 229–234.

[12] J.G. Lu, Z.Z. Ye, Y.J. Zeng, L.P. Zhu, L. Wang, J. Yuan, Q.L. Liang, Structural, optical, and electrical properties of (Zn, Al) O films over a wide range of com- positions, J. Appl. Phy. 100 (2006) 073714.

[13] Z.K. Heiba, L. Arda, Structural properties of Zn1-xMgxO nanomaterials pre- pared by sol-gel method, Cry. Res. Techn 44 (2009) 845–850.

[14] T. Fukumura, J. Zhengwu, A. Ohtomo, H. Koinuma, M. Kaisaki, An oxidediluted magnetic semiconductor: Mn-doped ZnO, Appl. Phys. Lett. 75 (1999) 3366.

[15] N. Dogan, A. Bingolbali, L. Arda, Preparation, structure and magnetic character- ization of Ni doped ZnO nano-particles, J. Magnet. Magnet. Mat. 373 (2015) 226–230.

[16] K. Ueda, H. Tabata, T. Kawai, Magnetic and electric properties of transition-metal- doped ZnO films, Appl. Phys. Lett. 79 (2001) 988.

[17] K. Koike, K. Hama, I. Nakashima, G. Takada, M. Ozaki, K. Ogata, S. Sasa, M. Inoue, M. Yano, Molecular beam epitaxial growth of wide band gap ZnCuO alloy films on (111)-oriented Si substrate toward UV-detector applications, Jpn. Jrn. Appl. Phy 43 (2004) 1372.

[18] Z.K. Heiba, L. Arda, M.B. Mohammed, Y.M. Nasser, N. Dogan, Effect of annealing temperature on structural and magnetic properties of Zn0.94Co0.05Cu0.0O, J. Supercond. Nov. Magn. 26 (2013) 3487.

[19] Y. Choi, J. Kang, D. Hwang, S. Park, Electron devices, recent advances in ZnO-based light-emitting diodes, IEEE Trans. Electron Devices 57 (2010) 26.

[20] M. Tosun, S. Ataoglu, L. Arda, O. Ozturk, E. Asikuzun, D. Akcan, O. Cakiroglu, Structural and mechanical properties of ZnCuO nanoparticles, Mater. Sci. Eng. A 590 (2014) 416–422.

[21] A. Ohtomo, M. Kawasaki, T. Koida, K. Masubuchi, H. Koinuma, Y. Sakurai, Y. Yoshida, T. Yasuda, Y. Segawa, $Cu_xZn_{1-x}O$ as a II–VI wide gap semiconductor alloy, Appl. Phys. Lett. 72 (1998) 2466.

[22] J.K. Salem, T.M. Hammad, The effect of surfactants on the particle size and optical properties of precipitated ZnO nanoparticles, J. Mater. Sci. Eng. 3 (2009) 38.

[23] B.D. Aleksandra, X.Y. Chen, Y.H. Leung, Nickel-zinc mixed metal oxide: copreci- pitation synthesis and application as gas sensors, Mater. Chem. 22 (2012) 6526–6535.

[24] I.P. Duru, C. Deger, T. Kalayci, M. Arucu, A computational study on magnetic effects of ZnCrO type diluted magnetic semiconductor, J. Magn. Magn. Mater. 396 (2015) 268.

[25] X.X. Liu, F.T. Lin, L.L. Sun, W.J. Cheng, X.M. Ma, W.Z. Shi, Doping concentration dependence of room-temperature ferromagnetism for Ni-doped ZnO thin films prepared by pulsed-laser deposition, Appl. Phys. Lett. 88 (2006) 062508.

[26] M. Venkatesan, C.B. Fizgerald, J.G. Lunney, J.M.D. Coey, Anisotropic ferro- magnetism in substituted zinc oxide, Phys. Rev. Lett. 93 (2004) 177206.

[27] T. Dietl, H. Ohno, F. Matsukura, J. Cibert, D. Ferrand, Zener model description of ferromagnetism in zinc-blende magnetic semiconductors, Science 287 (2000) 1019.

[28] K. Sato, H. Katayama-Yoshida, Material design for transparent Ferromagnets with ZnO-based magnetic semiconductors, J. Appl. Phys. 39 (2000) 555.

[29] K. Sato, H. Katayama-Yoshida, Material design of GaN-Based ferromagnetic diluted magnetic semiconductors, J. Appl. Phys. 40 (2001) 334.

[30] D.W. Wu, M. Yang, Z.B. Huang, G.F. Yin, X.M. Liao, Y.Q. Kang, X.F. Chen, H. Wang, Preparation and properties of Ni-doped ZnO rod arrays from aqueous solution, J. Colloid Interface Sci. 330 (2009) 380.

[31] S. Ghosh, P. Srivastava, B. Pandey, M. Saurav, P. Bharadwaj, D.K. Avasthi, D. Kabiraj, S.M. Shivaprasad, Study of ZnO and Ni-doped ZnO synthesized by atom beam sputtering technique, Appl. Phys. A. 90 (2008) 765.

[32] C.W. Cheng, G.Y. Xu, H.Q. Zhang, Y. Luo, Hydrothermal synthesis Ni-doped ZnO nanorods with room-temperature ferromagnetism, Mater. Lett. 62 (2008) 1617.

[33] L. Arda, M. Açıkgöz, N. Doğan, D. Akcan, O. Çakıroğlu, Synthesis, characterization and ESR studies of Zn1-xCoxO nanoparticles, J. Supercond. Nov. Magn. 27 (2014) 799–804.

[34] M. Ashokkumar, S. Muthukumaran, Microstructure, optical and FTIR studies of Ni, Cu co-doped ZnO nanoparticles by co-precipitation method, Opt. Mat. 37 (2014) 671–678.

[35] D. Theyvaraju, S. Muthukumaran, Preparation, structural, photoluminescence and magnetic studies of Cu doped ZnO nanoparticles co-doped with Ni by sol–gel method, Phys. E. 74 (2015) 93–100.

[36] L. Arda, M. Açıkgöz, A. Güngör, Magnetic and microstructure properties of Ni-doped ZnO films and powder by sol–gel process, J. Supercond. Nov. Magn. 25 (2012) 2701–2705.

[37] N. Doğan, A. Bingölbali, L. Arda, Preparation, structure and magnetic characterization of Ni doped ZnO nano-particles, J. M. M. M 373 (2015) 226–230.

[38] G. Gottstein, Physikalische Grundlagen der Materialkunde, 4th Edition (Berlin, Heidelberg, 2014, pp. 1–4.

[39] A.L. Taylor, G. Filipovich, G.K. Lindeberg, Electron paramagnetic resonance associated with Zn vacancies in neutron-irradiated ZnO, Solid State Commun. 8 (17) (1970) 1359–1361.

[40] D. Galland, A. Herve, ESR spectra of the zinc vacancy in ZnO, Phys. Lett. A 33 (1) (1970) 1–2.

[41] R. Elilarassi, G. Chandrasekaran, Structural, optical and magnetic charazterization of Cu-Doped ZnO nanoparticles synthesized using solid state reaction method, J. Matter Sci.: Matter Electron 21 (2010) 1168–1173, https://doi.org/10.1007/s10854-009-0041-y.

[42] J.A. Wibowo, N.F. Djaja, R. Saleh, Cu- and Ni-doping effect on structure and magnetic properties of Fe-doped ZnO nanoparticles, Adv. Mater. Phys. Chem. 3 (2013) 48–57., https://doi.org/10.4236/ampc.2013.31008.